Surface brightness of dark matter: Unique signatures of neutralino annihilation in the galactic halo

Carlos Calcáneo-Roldán* and Ben Moore†
Department of Physics, Durham University, Science Laboratories, Durham DH1 3LE, United Kingdom
(Received 19 June 2000; published 27 November 2000)

We use high resolution numerical simulations of the formation of cold dark matter halos to simulate the background of decay products from neutralino annihilation, such as gamma-rays or neutrinos. Halos are non-spherical, have steep singular density profiles and contain many thousands of surviving dark matter substructure clumps. This leads to several unique signatures in the gamma-ray background that may be confirmed or rejected by the next generation of gamma-ray experiments. Most importantly, the diffuse background is enhanced by over two orders of magnitude due to annihilation within substructure halos. The largest dark substructures are easily visible above the background and may account for the unidentified Energetic Gamma Ray Experiment Telescope (EGRET) sources. A deep strip survey of the gamma-ray background would allow the shape of the galactic halo to be quantified.

PACS number(s): 98.35.Gi, 95.35.+d, 95.75.Pq, 95.85.Pw

I. INTRODUCTION

Determining the nature of dark matter is of fundamental importance to both astronomy and particle physics. Both theory and observational data currently favor a universe with a matter density that is dominated by non-baryonic particles. Many candidates have been proposed: some are known to exist, others are more speculative (e.g., Ref. [1] and references therein). Structure formation in a universe dominated by cold dark matter (CDM) has been extensively tested against observations, and the model has proven highly successful at reproducing the large scale properties and distributions of galaxies [2,3]. On the nonlinear scales of galactic halos, it remains to be confirmed whether the model can successfully reproduce the observational data [4–6].

Direct detection in the laboratory is the ultimate technique for verifying the existence of dark matter particles (see, Ref. [7]). However, even the most popular candidate for dark matter, the neutralino, has a cross section that spans many orders of magnitude, and the current laboratory searches are only just becoming sensitive to the cosmologically interesting parameter range. Presently, astronomical observations provide the best insights into the nature of the dark matter. Furthermore direct detection relies on the existence of a smooth component of dark matter.

Within the next few years indirect detection of neutralinos will provide interesting constraints on their possible cross-sections and masses. Neutralino-neutralino annihilation produces observable photons (as well as a host of other particles) that may be observed as a diffuse gamma-ray background from the halo surrounding the Milky Way as discussed in Refs. [8–14] and, more recently, in Refs. [15–19].

Renewed interest in these predictions has recently arisen because of an unexplained component of diffuse high energy photons in the Energetic Gamma Ray Experiment Telescope (EGRET) data (e.g. Ref. [20]), and also the possibility of an excess from the center of the Galaxy itself [21], unexpected clumpy emissions and the unresolved discrete sources [22]. Progress in this area will result from several new and sensitive gamma-ray surveys such as the Gamma Ray Large Area Space Telescope (GLAST) [23] and the Very Energetic Radiation Imaging Telescope Array (VERITAS) [24].

The efficiency of the annihilation process is strongly dependent on both the local density and the cross-section of the neutralino. Many authors have calculated the expected flux from the galactic halo using simple models for the expected mass distribution of neutralinos within the Galaxy (see, e.g., Refs. [16,18]) or from its satellites [14,19].

Advances in computational cosmology have lead to several recent breakthroughs that have direct relevance to the detection of dark matter. In particular, the numerical resolution that can be achieved using parallel computational techniques is now sufficient to study the internal structure of dark matter halos that form within a cosmological context. The results of these simulations have important implications for indirect (and direct) detection of dark matter candidates. Most significantly for particle-particle annihilation, we are now confident that the central density profile of CDM halos follows a singular power law down to small scales [25–28]. Thus we may expect a point like source of mono-chromatic gamma-rays emanating from the center of the Milky Way, where the annihilation rate will be very high.

A second fundamental prediction of the CDM model is that previous generations of the merging hierarchy survive within halos [28]. Halos that accrete into larger systems may be tidally stripped of most of their mass. However their dense central cores survive and continue to orbit within the parent halos. This may present some problems for the CDM model since the predicted number of satellites within the Milky Way's halo is 50–100 times as many as observed [5]. If the CDM model is correct, then only a fraction of these satellites must have formed stars, and most of the substruc-

*Email address: c.a.calcaneo-roldan@durham.ac.uk
†Email address: ben.moore@durham.ac.uk

ture remains as dark objects within the galactic halo.

The possibility of an enhanced gamma-ray background from dark matter substructure was explored by Bergström *et al.* [29], who made simple assumptions as to the mean density and abundance of such clumps. We can now use the high resolution *N*-body simulations to directly measure these quantities. The simulations also allow us to study the influence of the halo shapes on the diffuse gamma-ray background, as well as the intensity of the central halo emission that arises from the singular dark matter density profiles. This paper is organized as follows: In Sec. II we explore the gamma-ray background that results from the smoothly distributed component of dark matter using both analytical and simulated halos. In Sec. III we focus on the substructure within halos. Our conclusions are summarized in Sec. IV.

II. THE SKY DISTRIBUTION OF THE GAMMA-RAY BACKGROUND

In what follows we will consider a flux of photons (or other particles) that are a by-product of the annihilation of dark matter particles within the smooth component of dark matter that surrounds the Galaxy. It is not our intention to discuss the details of neutralino interactions, since a complete overview on these processes (and supersymmetric matter in general) can be found in Refs. [30,31].

A. Model neutralino halos

We calculate the gamma-ray flux along a given line of sight through a spherically symmetric galactic halo using

$$\phi(\psi)=\frac{K}{4\pi}\int_{Line\ of\ sight}\rho^2(l)dl(\psi) \tag{1}$$

where ψ is the angle between the direction of galactic center and observation, and ρ, is the density of dark matter at distance l from the observer. We have summed up the dependence of the flux on neutralino mass and interaction cross sections in the constant K. This is enough scope for the present discussion—it is straightforward to take our results and input a neutralino cross-section, $\langle\sigma v\rangle$, and mass, M_χ, to determine the absolute gamma-ray flux (where K is defined to be $\langle\sigma v\rangle/M_\chi^2$). Our results can also be used to infer the sky distribution of other products of the annihilation, such as neutrinos or positrons.

The line of sight distance, l, is related to the radial distance from the halo center, r, via

$$r^2=l^2+R_o^2-2lR_o\cos(\psi)$$

where R_o is our galacto-centric distance, taken here to have the IAU standard value of $R_o=8.5$ kpc (kiloparsec) [32], and ψ is related to galactic coordinates (ℓ,b) through

$$\cos(\psi)=\cos(\ell)\cos(b).$$

For the halo density profile, $\rho(r)$, we take the latest results from the highest resolution numerical simulations of galactic halos carried out to date [5]. These authors simulated 6 different galactic mass halos with force resolution of 0.5 kpc and mass resolution of $10^6 M_\odot$. (Throughout the paper we will use the Hubble constant value of $H_o=100\,h\ \mathrm{km\,s^{-1}\,Mpc^{-1}}$, and $h=0.5$, as adopted for the simulations.) The best fitting density profile to this data is (subscript *moore*)

$$\rho_{moore}(r)=\frac{\rho'_{moore}}{(r/a)^{1.5}(1+(r/a)^{1.5})} \tag{2}$$

where r is the distance from the halo center and $a=r_{200}/c_{moore}$, the scale radius for halos of mass $\approx 1\times10^{12}\ M_\odot$. The virial radius of our fiducial galactic halo, $r_{200}\approx 300$ kpc, is defined as the radius of a sphere at which the mean overdensity is 200 times the cosmological mean density. (A central density profile of slope -1.5 on galactic scales was also found by Jing and Suto [33], and confirmed as an asymptotic slope by Ghigna *et al.* [34].)

We also compare this profile with that determined by Navarro, Frenk and White (NFW) [26] using a sequence of lower resolution studies (subscript nfw) (the main difference being that the central dark matter density profile has a slope of -1):

$$\rho_{\mathrm{nfw}}(r)=\frac{\rho'_{\mathrm{nfw}}}{(r/a)(1+r/a)^2} \tag{3}$$

and the modified isothermal profile with a constant density core (subscript *is*):

$$\rho_{is}(r)=\frac{\rho'_{is}}{[1+(r/a)^2]^{3/2}}. \tag{4}$$

The scale radius, a, is determined directly from the numerical simulations, except for the modified isothermal model which we normalize to match the observational rotation curve data (as in Ref. [35]); $a_{is}=24.3$ kpc, $a_{\mathrm{nfw}}=27.7$ kpc and $a_{moore}=33.2$ kpc (this radius is directly related to the concentration parameter, $c=r_{200}/a$). We normalize each density profile such that the peak circular velocity, $v_{peak}=200\ \mathrm{km\,s^{-1}}$ (the maximum of the $v_c=\sqrt{GM/r}$ curve), which gives $\rho'_{is}=4.96\times10^6\,M_\odot\,\mathrm{kpc}^{-3}$, $\rho'_{\mathrm{nfw}}=5.11\times10^6\,M_\odot\,\mathrm{kpc}^{-3}$ and $\rho'_{moore}=1.64\times10^6\,M_\odot\,\mathrm{kpc}^{-3}$. We plot the effective circular velocity profiles and density profiles of these model halos in Fig. 1(a) and Fig. 1(b), respectively.

In Fig. 2 we plot the flux, ϕ, along the line of sight through a spherical Milky Way halo using the above density profiles as the observer looks towards the galactic center, at $\psi=0°$, to the galactic anticenter, at $\psi=180°$. As expected, the central annihilation flux depends strongly on the form of the inner density profile. At an angle of five degrees from the galactic center, the ratio of fluxes from the three different profiles, *moore:nfw:is*, is 1000:100:1.

The peak central value depends upon the distance from the galactic center that we are willing to consider integrating

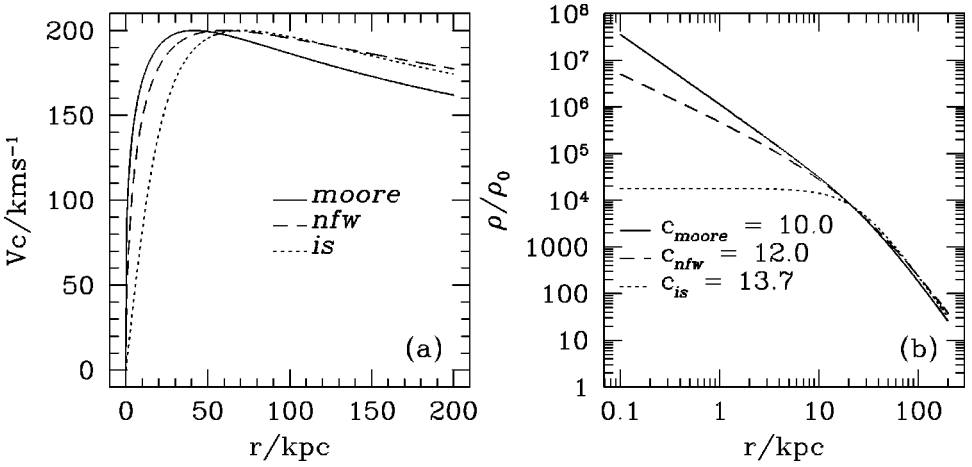

FIG. 1. (a) The circular velocity curves $V_c(r)=\sqrt{GM(r)/r}$, and (b) density profiles are plotted as a function of the radius for each of the halo models considered in the text.

from—the flux slowly diverges for the density profile in Eq. (2). However, within a given radius, most of the neutralinos would have self annihilated, leaving a tiny constant density core. We can estimate the size of this core using $(n\sigma v)^{-1}=t_h$, where $t_h\sim 10$ Gyrs is the Hubble time. Taking a typical cross section, $\sigma v=10^{-30}\,\mathrm{cm}^3\,\mathrm{s}^{-1}$, and adopting the Moore *et al.* density profile, we find that the annihilation radius within the Milky Way is approximately 4×10^{-7} parsecs $\approx 10^{-12}\,r_{200}$.

The total flux that arises within 5 degrees of the galactic center using the Moore *et al.* density profile is a factor of 20 larger than that found using the NFW profile (both integrated down to the annihilation radius calculated above).

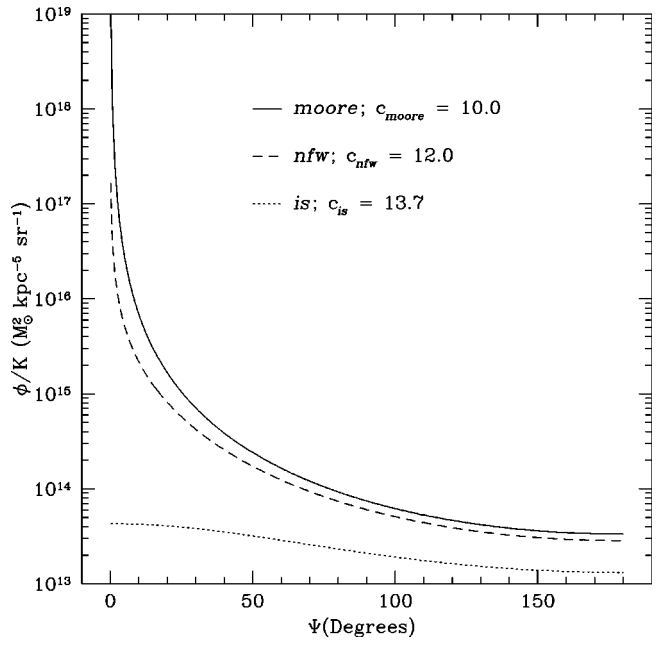

FIG. 2. The gamma ray flux from neutralino annihilation, $\phi(\psi)$, plotted as a function of the angular distance from the galactic center ψ. The curves show the results using the three different density profiles plotted in Fig. 1. The flux at a given position is averaged over 4π steradians.

B. Comparison with high resolution CDM simulations

We can use the numerical simulations to compare directly with the above predictions that were obtained assuming spherical symmetry. We refer the reader to Moore *et al.* (Ref. [5]) for details of the numerical simulations.[1] To construct the expected gamma-ray sky maps, we choose a simulated dark matter halo at a redshift $z=0$ that has a peak circular velocity of $\sim 200\,\mathrm{km\,s}^{-1}$ and a total mass, within the virial radius $r_{200}=300$ kpc, of $1\times10^{12}\,M_\odot$. This simulated halo is from the local group simulation and is close to our fiducial Milky Way cold dark matter halo that we adopted in the previous section.

N-body simulations attempt to simulate a collisionless fluid of dark matter using discrete massive particles. We calculate the local density at the position of each particle by averaging over its nearest 64 neighbors. The observer is placed 8.5 kpc from the halo center (defined using the most bound particle in the simulation) and we sum up the flux of annihilation products along each line of sight using the discrete equivalent to Eq. (1):

$$\Phi(\ell,b)=\frac{K}{\Omega}\sum_{LOS}\rho_i^2(\ell,b)\Delta r_i(\ell,b) \qquad (5)$$

where ℓ,b are galactic longitude and latitude, respectively. The flux is binned in angular windows of size $\Omega=1^\circ\times1^\circ$, and in the radial direction in fixed increments $\Delta r_i=1$ kpc.

The simulated dark matter halos are typically flattened oblate or prolate systems [36]. We do not know *a priori* in which axis the stellar disk would be located. Therefore we show two all-sky maps using the same dark matter halo but viewed using two different locations for the observer: Fig. 3(a) and Fig. 3(b) have the observer located on the short and long axes, respectively. Both of these plots show the enhanced brightening towards the halo center, as well as some clumpy substructure in the halo itself. Note that both the central halo and the centers of the substructure halos are

[1]Images, data and movies of these dark matter simulations can be downloaded from http://www.nbody.net

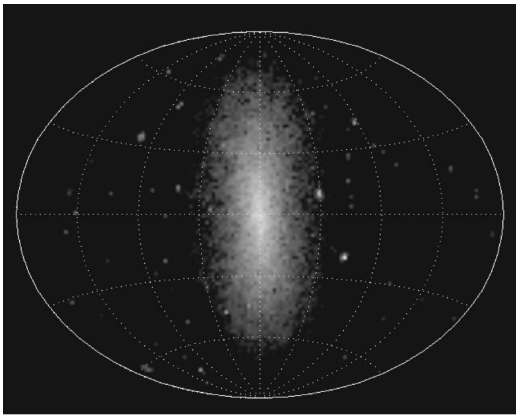

(a)

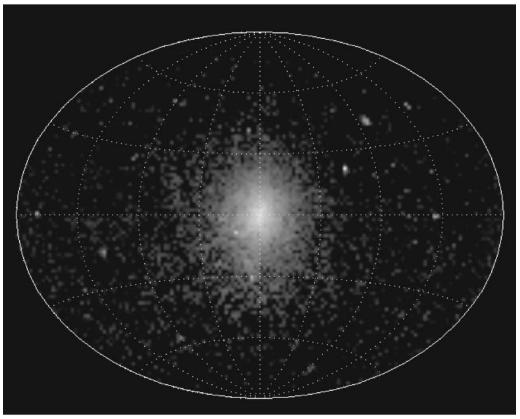

(b)

FIG. 3. All-sky maps of the gamma ray background constructed using a single high-resolution *N*-body simulation of a cold dark matter halo. The observer has been placed in the short (a) and long (b) axis of the simulated halo.

artificially dimmed in these plots due to the numerical resolution ~ 0.5 kpc, which sets a maximum density that can be resolved. The non-spherical shape of the halo is also clearly evident by inspecting the plots with different observer positions.

Recent estimates for the shape of the Milky Way's halo (see, e.g., [37] and references therein), suggest that it may be flattened with a short/long axis ratio of 0.5. An independent estimate from the orbit of the Sagittarius debris stars yields a nearly spherical dark matter halo [38]. The simulated halo that we have chosen to analyze represents a typical prolate CDM halo with a short to long axis ratio of 0.4, and an intermediate to long axis ratio of 0.5.

It is straightforward to estimate the effects of flattened dark matter halos by modifying Eq. (1) to accommodate triaxial shaped bodies. The simplest way to achieve this is to change from spherical coordinate r to

$$\xi^2 = \frac{x^2+y^2}{b^2} + \frac{z^2}{c^2}$$

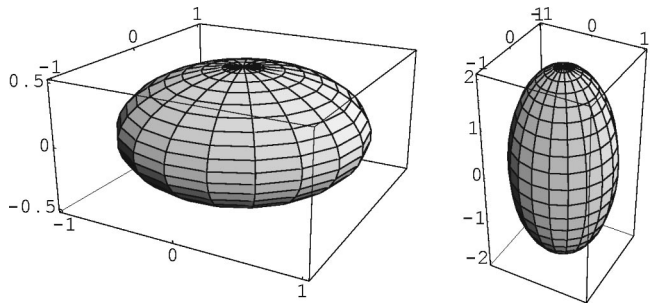

FIG. 4. The left panel shows a unit oblate ellipsoid and the right hand panel shows a unit prolate ellipsoid. The axial ratios for both are 2:1.

where $b>c$ for the oblate case, $b<c$ for the prolate and we leave z as the axis of symmetry. A 2D visualization of these 3D shapes is illustrated in Fig. 4.

In Fig. 5 we plot spherical, oblate (2:1) and prolate (2:1) versions of the integral in Eq. (1) using the Moore *et al.* (1999) density profile. The observer is located on a plane parallel to the axis of symmetry, again at a distance $R_o = 8.5$ kpc from the center of the halo. The halo shape leads to little difference towards the galactic center, but at the anti-center prolate, halos can be 100 times brighter than oblate halos.

We can also compare the predicted angular flux with that measured directly from the *N*-body simulation. The annihilation flux is averaged in ten degree bins from the simulated dark matter halo, along a great circle from the galactic center to its anti-center. This direct measurement of the flux is also plotted (as points) in Fig. 5. This data is particularly noisy

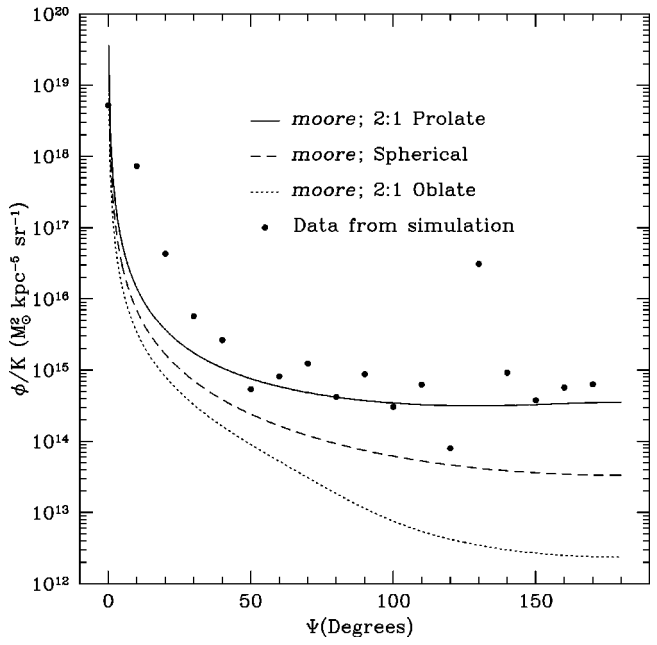

FIG. 5. The gamma ray flux, ϕ, plotted as a function of angle ψ, for smooth halos of the same total mass using the density profile given in Eq. (2) for spherical, oblate and prolate halo geometries. The points are values of the flux measured directly from the *N*-body halo illustrated in Fig. 3.

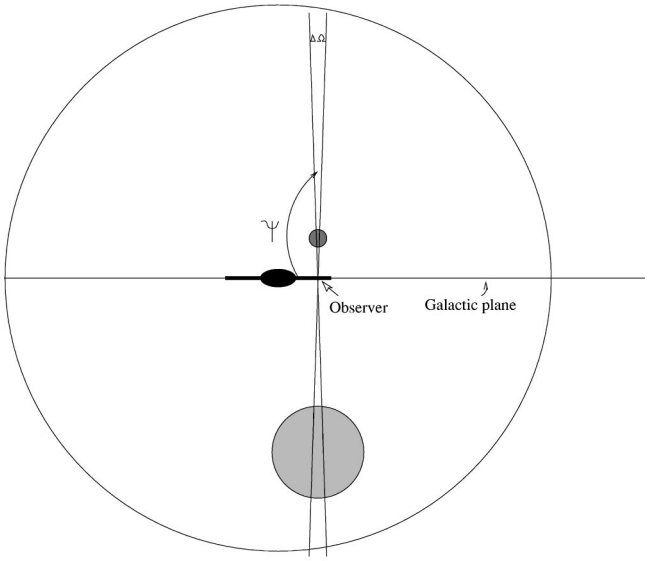

FIG. 6. A sketch showing the geometry of an observer in the galaxy viewing substructure in the galactic halo.

due to the large numbers of substructure clumps in the simulation—the spike at $\psi = 125°$ is due to a massive dark clump that happens to lie exactly along this chosen line of sight.

III. SUBSTRUCTURE

A. Enhancement of global flux due to substructure

Cold dark matter substructure clumps have singular density profiles that will be a significant source of annihilation products. The velocities and spatial distribution of dark matter substructure is unbiased with respect to the smooth dark matter background [34]. Therefore, to first order, substructure increases the global sky brightness in any given direction. However, the details depend on how much substructure survives within the solar radius and also on how far down the mass function substructure halos form and survive.

First we will estimate the annihilation flux from clumps of dark matter that are known to exist in the galactic halo, *i.e.* the dark matter halos that surround the Magellanic Clouds and dwarf spheroidal galaxies. In fact, high-energy gamma-ray emissions from the Large Magellanic Cloud (LMC) were detected with EGRET by Sreekumar *et al.* [39] in 1992 (although the origin of this emission was reported to be the interaction of cosmic rays with interstellar matter).

We estimate the average flux, Φ_{AV}, from the dark matter halos that surround some of the principal structures in the local group: The Andromeda Galaxy, M31 ($v_{peak} = 200$ km s^{-1} at a distance of 700 kpc), The Large and Small Magellanic Clouds ($v_{peak} = 70$ km s^{-1} and $v_{peak} = 40$ km s^{-1}, respectively, both at a distance of 50 kpc), Draco ($v_{peak} = 10$ km s^{-1} at a distance of 50 kpc) and a small dark matter clump ($v_{peak} = 2$ km s^{-1} at a distance of 10 kpc). A sketch of the geometry is given in Fig. 6.

The total flux from a substructure halo at distance R_c from the observer is

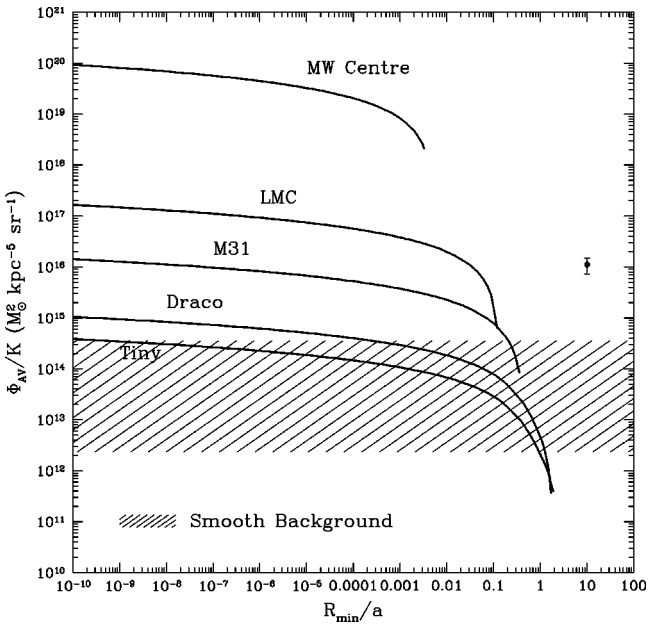

FIG. 7. The gamma ray flux, Φ_{AV}, plotted as a function of minimum integration radius R_{min} for halo substructure of different circular velocities and distances as detailed in the text. The shaded region shows the range of background values at the galactic anti-center that can be expected depending on the halo shape. The point is the average flux due to all clumps with $v_{peak} > 1$ km s^{-1}. Note that the size of the error bar on this point depends on the area of the sky surveyed.

$$\Phi_{TOT}(R_c) = \frac{K}{R_c^2} \int \rho^2(r) r^2 dr. \tag{6}$$

By considering the central $\Delta\Omega = 1° \times 1°$ patch over each clump, we define the maximum integration limit in Eq. (6), and the average flux is then

$$\Phi_{AV} = \frac{\Phi_{TOT}}{\Delta\Omega} \tag{7}$$

(we set $\Delta\Omega$ in steradians so we may compare it directly with the smooth flux of Sec. II).

For the dark matter distribution within the substructure clumps we use the Moore *et al.* profile, which provides a good fit to the smallest, well-resolved substructure halos. The concentration of CDM halos is a function of mass [40], and for the density profile in Eq. (2), this can be written

$$c_{moore} \approx 102 \left(\frac{M_{vir}}{1 h^{-1} M_\odot} \right)^{-0.084}. \tag{8}$$

This defines the scale radius of each substructure clump: $a_{\rm M31} = 33.3$ kpc, $a_{\rm LMC} = 6.7$ kpc, $a_{\rm SMC} = 3.1$ kpc, $a_{\rm Draco} = 0.5$ kpc, and $a_{\rm Tiny} = 0.05$ kpc.

The integral in Eq. (6) diverges as $r \to 0$ for the density profile that we are using. However, even the smallest substructure halos will have a maximum density set by the ra-

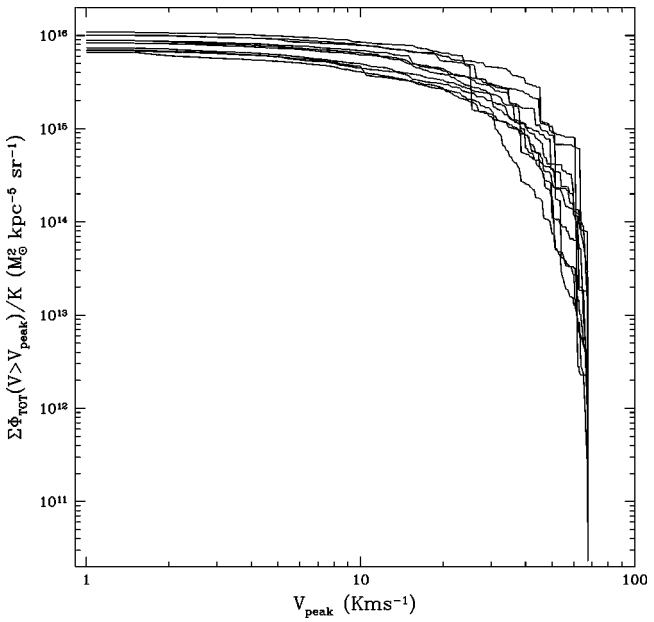

FIG. 8. The cumulative gamma-ray flux from halo substructures, $\Sigma\phi_{TOT}(v>v_{peak})$, above a given substructure circular velocity v_{peak}. The ten different curves correspond to different Monte Carlo realizations of a galactic halo of substructure halos. The flux is averaged over 4π steradian and can be compared with the flux from the smooth halo from Figs. 2 and 5.

dius within which most of the neutralinos would have self annihilated. We therefore present results for the average flux from these clumps as a function of the minimum integration radius R_{min}/a in Fig. 7, where a is the scale radius as defined above.

For comparison, we plot the range of background emission at the galactic anti-center as the shaded line in Fig. 7. The tiny clump is only marginally visible above the background flux (depending on whether or not the galactic halo is prolate or oblate), whereas most of the subhalos are easily visible. Also for comparison, we have plotted the flux from the inner region of the galaxy, which is the brightest of these sources.

Although the galactic halo is expected to contain just a few clumps more massive than the Magellanic Clouds, there are many thousands of smaller mass objects. The mass function of substructure is a power law close to $dn(m)/dm \propto m^{-1.9}$, or in terms of circular velocity, $dn(v_c)/dv_c \propto v_c^{-3.8}$ [34]. Above a circular velocity $v_{peak}=10\ \mathrm{km\,s^{-1}}$ and $1\ \mathrm{km\,s^{-1}}$, we expect the galactic halo to host roughly 1000 and 5×10^5 substructure halos, respectively. Future simulations should be able to measure how far down the mass function substructure halos can survive, as well as to determine their central density profiles. (We note that the highest resolution simulation to date resolved the substructure within a dark matter mini-halo of mass $10^7\,M_\odot$. The force resolution was 10 parsecs and the mass resolution was $10\,M_\odot$, allowing substructure with peak circular velocities as low as a few hundred meters per second to be resolved. The survival of substructure continues even down to this scale, where the slope of the power spectrum is close to -3.)

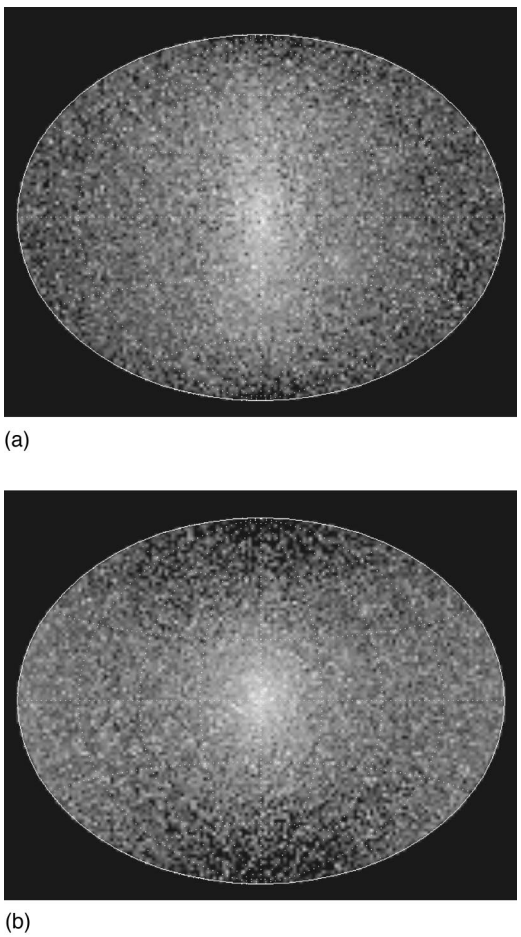

FIG. 9. All-sky map of the gamma ray background that arises solely from dark matter substructures. The positions and circular velocities of sub-halos above a circular velocity of $1\ \mathrm{km\,s^{-1}}$ are drawn from the *N*-body simulations, but the flux from each halo is calculated analytically. The observer is located on the short (a) and long (b) axis of symmetry. The grey scale corresponds to the log of the flux of annihilation products.

We calculate the total flux from substructure using Monte Carlo techniques. First we generate a list of peak circular velocities and positions of 5×10^5 substructure halos in the range of $1-70\ \mathrm{km\,s^{-1}}$. (Distances are randomly selected using the Moore *et al.* density profile, and peak circular velocities are randomly assigned from a power law distribution scaling as $v^{-3.8}$). For each lump, we estimate its total flux as in the previous cases, integrating Eq. (6) with a density profile scaled, according to Eq. (8), for the concentration.

In the absence of further constraints on the possible value for R_{min}, we use the same criteria as before and choose it to be a fixed fraction of the virial radius, $R_{min}\approx10^{-12}r_{200}$. This corresponds to a mean density of $\approx10^{22}\,M_\odot\,\mathrm{kpc^{-3}}$ for the galactic halo. The results are not too sensitive to the value of the minimum integration radius, as is apparent from inspection of Fig. 7. The total flux is then averaged over the entire sky and we repeat this process in order to estimate the variance. The cumulative distribution of flux above a given substructure peaks circular velocity ($\Sigma\Phi_{TOT}$) is plotted for ten of these random halo realizations in Fig. 8.

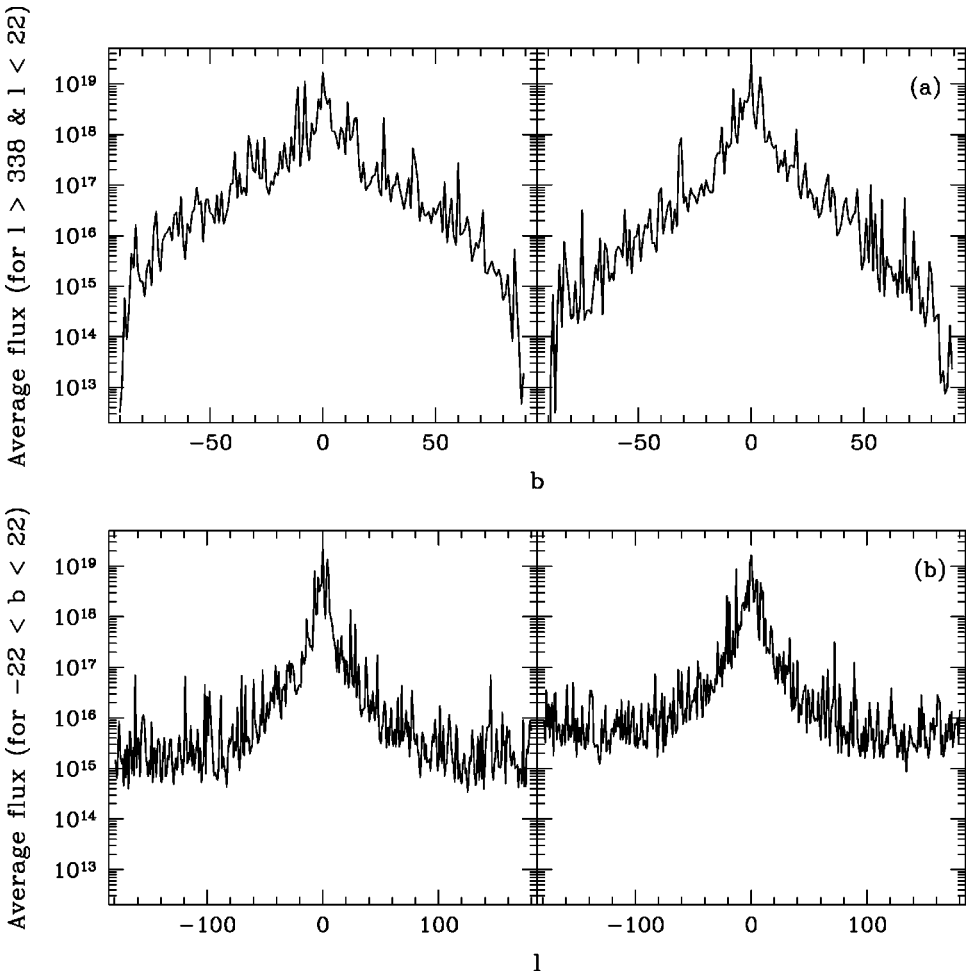

FIG. 10. The average gamma-ray flux per square degree from dark matter substructure as measured within the simulated CDM halo along a great circle of constant galactic latitude (a) and longitude (b). The average has been taken over a strip of width 44 degrees. The left hand plot represents the view along the short axis, while the right hand side is the view along the long axis.

It is evident from this plot that the effects of including the entire mass spectrum of substructure is quite dramatic, and boosts the expected flux from the smooth halo by several orders of magnitude. However, most of the flux arises from the subhalos with circular velocities larger than 10 $\mathrm{km\,s^{-1}}$. Extrapolating to very small halos would not change the total flux by a large factor.

To quantify the brightening of the background due to substructure, we have to calculate the average flux due to all clumps with $v_{peak} > 1\ \mathrm{km\,s^{-1}}$ within a spherical halo. The point plotted in Fig. 7 represents this contribution to the flux, where the error bar is the 1σ variation among the different Monte Carlo models. From this plot we see that the flux due to substructure is over two orders of magnitude brighter than the smooth background from a spherical halo. We note that one needs to observe a fairly large fraction of the sky (>100 square degrees) to ensure a significant number of clumps lie in the field of view. (Also note that the variance at high peak circular velocities is due to the proximity of the largest few dark matter substructures. However, the mean total flux converges to similar values for each Monte Carlo model.)

B. The flux due to substructure in prolate and oblate halos

Not only is the mean flux at a given position on the sky dominated by substructure halos, the spatial distribution of the flux across the sky will be determined by the substructure. The convergence study by Ghigna *et al.* [34] shows that substructure halos trace the global mass distribution of the halo. Therefore, we can use the *N*-body simulations to generate Monte Carlo distributions of substructure halos and construct all-sky maps of the expected gamma-ray flux. We take a random particle from the simulation and assign a circular velocity from a distribution $dn(v_c)/dv_c \propto v_c^{-3.8}$. For each sub-halo we calculate its total annihilation flux and then repeat the process until we have 500 000 halos above a circular velocity of 1 $\mathrm{km\,s^{-1}}$.

Figure 9(a) and Fig. 9(b) show the resulting sky distribution of flux from sub-halos binned in one degree bins, where the observer has been placed in the short and long axis of the simulation, respectively. Large substructure halos, such as the Magellanic Clouds in our own halo, will contain its own gravitationally bound sub-halos, which leads to clustering of gamma-ray emissions in the all sky maps.

Future observations may only be able to make deep strip maps. Therefore in Fig. 10, we have binned the flux along lines of constant galactic *l* and *b*, with the observer placed in the short and long axis of the global density distribution. From these plots we can see that the emission from substructure peaks at the galactic center, and as one would expect, this effect is not that much different for spherical halos than it is for prolate or oblate halos.

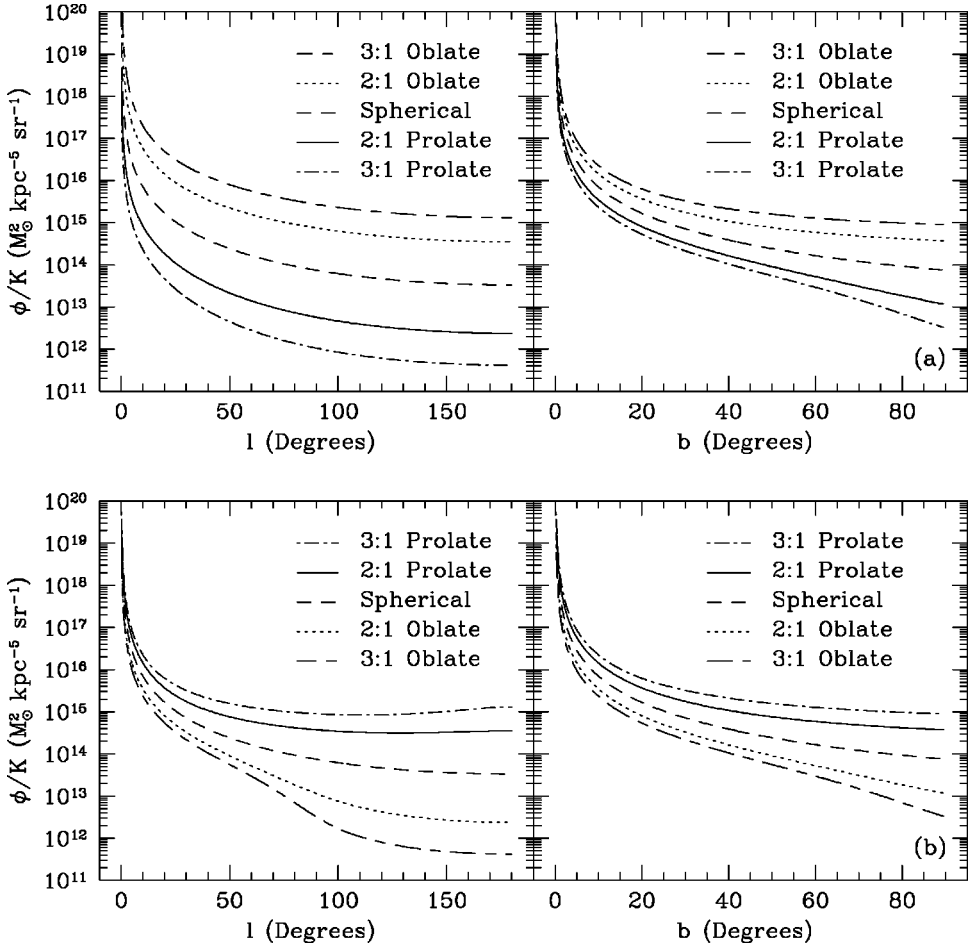

FIG. 11. The effect of halo shape on the gamma-ray flux. Halo density profiles are drawn from spherical, oblate or prolate distributions with the indicated axis ratios. The observer is placed in the short axis (a) while in (b) the observer is in the long axis.

Since the substructure traces the global mass distribution, a prolate halo would also have a prolate distribution of satellites. Therefore we can study the variation of flux within smooth prolate or oblate halos to examine how the background flux from substructure can be used to quantify the halo shape. We calculate the observed flux as a function l and b for spherical, prolate and oblate flattened 2:1 and 3:1 geometries. In each case, the density profile is taken from Eq. (2), and again the observer is placed in either the short [Fig. 11(a)] or long [Fig. 11(b)] axis of symmetry.

These plots show how the distribution of flux on the sky can vary significantly depending on the shape of the density distribution and on where the observer is situated within the halo.

C. The distribution of point sources

Individual substructures may be observed and quantified if the resolution of the telescope is sufficient. However, all of the past and present observations would only detect substructure as unresolved point sources. The distribution of their fluxes (and spatial distribution on the sky) may be used to rule out alternative origins, such as extra-galactic sources. In Fig. 12 we plot the cumulative distribution of point sources above a given flux within one degree square bins. The two curves consider substructure with peak circular velocities larger than 10 km s^{-1} and 1 km s^{-1}. The number density of the brightest sources in the sky scales as $N \propto F^{-0.7}$.

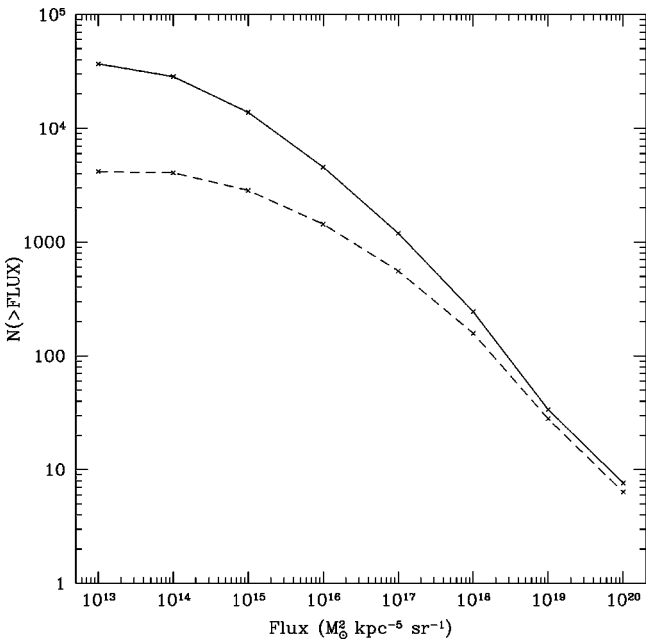

FIG. 12. The cumulative number of gamma-ray sources above a given flux within a window $\Delta\Omega = 1° \times 1°$. The two curves are for substructure halos with circular velocities larger than 10 km s^{-1} (dashed line) and 1 km s^{-1} (solid line).

Higher resolution simulations are vital to quantify how much substructure survives within the galactic halo, how it is spatially distributed and to quantify the internal structure of surviving substructure. However, Fig. 12 gives an idea of what to expect if an all sky survey that is capable of detecting the brightest substructure halos is carried out.

IV. CONCLUSIONS

Numerical simulations that follow the growth of structure within a universe dominated by neutralinos (cold dark matter) have achieved a resolution that allows their global structure and internal structure to be quantified. The density profiles, shapes of dark matter halos, and abundance and properties of dark matter substructure all play an important role in determining the absolute surface brightness of observable products from dark matter annihilation.

We have used the results from the highest resolution simulations ever performed of CDM halos to examine the expected all-sky distribution of gamma-rays from neutralino annihilation. Substructure can boost the expected flux significantly over that originating from a smooth dark matter halo. Thus, gamma-ray observations, such as EGRET data, may already have the potential of constraining a large part of the parameter range of the neutralino cross-sections. The distinguishing shapes of CDM halos, and the unique spatial and flux distribution of point sources from substructure within the galactic halo, should allow a unique identification of observational data with dark matter.

ACKNOWLEDGMENTS

The authors would like to thank Prof. Arnold Wolfendale for numerous discussions and suggestions that have improved the quality of this work. Carlos Calcáneo-Roldán continues his research thanks to the generous support from the People of México through a grant by CONACyT. Ben Moore thanks the Royal Society for financial support. Computations were carried out as part of the Virgo consortium.

[1] J. Ellis, Phys. Scr. **T85**, 221 (2000).
[2] M. Davis, G. Efstathiou, C. S. Frenk, and S. D. M. White, Astrophys. J. **292**, 371 (1985).
[3] C. M. Baugh, S. Cole, C. S. Frenk, and C. G. Lacey, Astrophys. J. **498**, 504 (1998).
[4] B. Moore, Nature (London) **370**, 629 (1994).
[5] B. Moore, S. Ghigna, F. Governato, G. Lake, T. Quinn, J. Stadel, and P. Tozzi, Astrophys. J. Lett. **524**, L19 (1999).
[6] A. A. Klypin, A. V. Kravtsov, O. Valenzuela, and F. Prada, Astrophys. J. **522**, 82 (1999).
[7] J. Collar, Phys. Rev. D **59**, 063514 (1999).
[8] J. E. Gunn, B. W. Lee, I. Lerche, D. N. Schramm, and G. Steigman, Astrophys. J. **223**, 1015 (1978).
[9] F. W. Stecker, Astrophys. J. **223**, 1032 (1978).
[10] J. Silk and M. Srednicki, Phys. Rev. Lett. **53**, 624 (1984).
[11] M. S. Turner, Phys. Rev. D **34**, 1921 (1986).
[12] J. Silk and H. Bloemen, Astrophys. J. Lett. **313**, L47 (1987).
[13] A. Bouquet, P. Salati, and J. Silk, Phys. Rev. D **40**, 3168 (1989).
[14] G. Lake, Nature (London) **346**, 39 (1990).
[15] L. Bergström, J. Edsjö, and P. Gondolo, Phys. Rev. D **58**, 103519 (1998).
[16] L. Bergström, P. Ullio, and J. H. Buckley, Astropart. Phys. **9**, 137 (1998).
[17] E. A. Baltz and J. Edsjö, Phys. Rev. D **59**, 023511 (1999).
[18] P. Gondolo and J. Silk, Phys. Rev. Lett. **83**, 1719 (1999).
[19] E. A. Baltz, C. Briot, P. Salati, R. Taillet, and J. Silk, Phys. Rev. D **61**, 023514 (2000).
[20] D. D. Dixon, D. H. Hartman, E. D. Kolaczyk, and J. Samimi, New Astron. **3**, 539 (1998).
[21] H. A. Mayer-Hasselwander, D. L. Bertsch, B. L. Dingus, A. Eckart, J. A. Esposito, R. Genzel, R. C. Hartman, S. D. Hunter, G. Kanbach, D. A. Kniffen, Y. C. Lin, P. F. Michelson, A. Muecke, C. von Montigny, R. Mukherjee, P. L. Nolan, M. Pohl, O. Reimer, E. J. Schneid, P. Sreekumar, and D. J. Thompson, Astron. Astrophys. **335**, 161 (1998).
[22] R. C. Hartman, D. L. Bertsch, S. D. Bloom, A. W. Chen, P. Deines-Jones, J. A. Esposito, C. E. Fichtel, D. P. Friedlander, S. D. Hunter, L. M. McDonald, P. Sreekumar, D. J. Thompson, B. B. Jones, Y. C. Lin, P. F. Michelson, P. L. Nolan, W. F. Tompkins, G. Kanbach, H. A. Mayer-Hasselwander, A. Mücke, M. Pohl, O. Reimer, D. A. Kniffen, E. J. Schneid, C. von Montigny, R. Mukherjee, and B. L. Dingus, Astrophys. J., Suppl. Ser. **123**, 79 (1999).
[23] N. Gehrels and P. Michelson, Astropart. Phys. **11**, 277 (1999).
[24] R. W. Lessard, Astropart. Phys. **11**, 243 (1999).
[25] R. G. Carlberg, Astrophys. J. **433**, 468 (1994).
[26] J. F. Navarro, C. S. Frenk, and S. D. M. White, Astrophys. J. **462**, 563 (1996).
[27] B. Moore, F. Governato, J. Stadel, T. Quinn, and G. Lake, Astrophys. J. Lett. **499**, L5 (1998).
[28] S. Ghigna, B. Moore, F. Governato, G. Lake, T. Quinn, and J. Stadel, Mon. Not. R. Astron. Soc. **300**, 146 (1998).
[29] L. Bergström, J. Edsjö, P. Gondolo, and P. Ullio, Phys. Rev. D **59**, 043506 (1999).
[30] G. Jungman, M. Kamionkowsky, and K. Griest, Phys. Rep. **267**, 195 (1996).
[31] L. Bergström, Nucl. Phys. B, Proc. Suppl. **70**, 31 (1999).
[32] F. J. Kerr and D. Lynden-Bell, Mon. Not. R. Astron. Soc. **221**, 1023 (1986).
[33] Y. P. Jing and Y. Suto, Astrophys. J. Lett. **529**, L69 (2000).
[34] S. Ghigna, B. Moore, F. Governato, G. Lake, T. Quinn, and J. Stadel, Astrophys. J. (to be published), astro-ph/9910166.
[35] A. V. Kravtsov, A. A. Klypin, J. S. Bullock, and J. R. Primack, Astrophys. J. **502**, 48 (1998).
[36] J. Barnes and G. Efstathiou, Astrophys. J. **319**, 575 (1987).
[37] R. P. Olling and M. R. Merrifield, Astron. Soc. Pac. Conf. Ser. **136**, 219 (1998).

[38] R. Ibata, G. F. Lewis, M. Irwin, E. Totten, and T. Quinn, astro-ph/0004011.

[39] P. Sreekumar, D. L. Bertsch, B. L. Dingus, C. E. Fichtel, R. C. Hartman, S. D. Hunter, G. Kanbach, D. A. Kniffen, Y. C. Lin, J. R. Mattox, H. A. Mayer-Hasselwander, P. F. Michelson, C. von Montigny, P. L. Nolan, K. Pinkau, E. J. Schneid, and D. J. Thompson, Astrophys. J. Lett. **400**, L67 (1992).

[40] A. Klypin, S. Gottlöber, and A. V. Kravtsov, Astrophys. J. **516**, 530 (1999).